

## Satellite-based estimation of surface vapor pressure deficits using MODIS land surface temperature data

Hirofumi Hashimoto<sup>a,b,\*</sup>, Jennifer L. Dungan<sup>c</sup>, Michael A. White<sup>d</sup>, Feihua Yang<sup>e</sup>, Andrew R. Michaelis<sup>a,c</sup>, Steven W. Running<sup>f</sup>, Ramakrishna R. Nemani<sup>c</sup>

<sup>a</sup> California State University, Monterey Bay, CA, USA

<sup>b</sup> Graduate School of Agricultural and Life Sciences, University of Tokyo, Tokyo, Japan

<sup>c</sup> NASA Ames Research Center, Moffett Field, CA, USA

<sup>d</sup> Department of Aquatic, Watershed, and Earth Resources, Utah State University, Logan, UT, USA

<sup>e</sup> Department of Geography, University of Wisconsin, Madison, WI, USA

<sup>f</sup> NTSG/University of Montana, Missoula, MT, USA

Received 21 March 2006; received in revised form 28 February 2007; accepted 21 April 2007

### Abstract

Vapor Pressure Deficit (VPD) is a principle mediator of global terrestrial CO<sub>2</sub> uptake and water vapor loss through plant stomata. As such, methods to estimate VPD accurately and efficiently are critical for ecosystem and climate modeling efforts. Based on prior work relating energy partitioning, remotely sensed land surface temperature (LST), and VPD, we developed simple linear models to predict VPD using saturated vapor pressure calculated from MODIS LST at a number of different temporal and spatial resolutions. We developed and assessed the LST–VPD models using three data sets: (1) instantaneous and daytime average ground-based VPD and radiometric temperature from the Soil Moisture Experiments in 2002 (SMEX02); (2) daytime average VPD from AmeriFlux eddy covariance flux tower observations; and (3) estimated daytime average VPD from Global Surface Summary of Day (GSSD) observations. We estimated model parameters for VPD estimation both regionally (MOD11 A2) and globally (MOD11 C2) with RMSE values ranging from .32 to .38 kPa. VPD was overestimated along coastlines and underestimated in arid regions with low vegetation cover. Also, residuals were larger with higher VPDs because of the non-linear function of saturation vapor pressure with LST. Linear relationships were seen at multiple scales and appear useful for estimation purposes within a range of 0 to 2.5 kPa.

© 2007 Elsevier Inc. All rights reserved.

**Keywords:** VPD; Land surface temperature; MODIS

### 1. Introduction

Vapor Pressure Deficit (VPD), the difference between saturated vapor pressure at air temperature and actual vapor pressure, is one of the most important climatic variables used in ecosystem models to simulate fluxes and states of water and carbon (Waring & Running, 1998). High VPD causes plants to reduce stomatal aperture to prevent excessive water loss, which in turn reduces CO<sub>2</sub> uptake for photosynthesis. VPD estimates

on a daily or weekly basis are used in models of carbon cycling by vegetation (e.g. Aber et al., 1996; Van Wijk et al., 2000; White et al., 2000) and are critical to the understanding of vegetation behavior under drought stress.

For regional and global ecosystem carbon and water modeling, the spatial pattern of meteorological variables usually is calculated through spatial interpolation of data from surface weather stations. These interpolation techniques, including Thiessen polygons (Thiessen, 1911), inverse-distance weighting (Watson & Philip, 1985), ordinary kriging (Brooker, 1979), truncated Gaussian filtering (Thornton et al., 1997), and thin plate splines (Hutchinson & Gessler, 1994), are suitable in situations where measurements are available at sufficient density. Mapping VPD with interpolation presents several challenges. First, the

\* Corresponding author. c/o Ramakrishna R. Nemani, MS 242-4, NASA Ames Research Center, Moffett Field, CA 94035-1000, USA. Tel.: +1 650 604 6446; fax: +1 650 604 6569.

E-mail address: [hirofumi.hashimoto@gmail.com](mailto:hirofumi.hashimoto@gmail.com) (H. Hashimoto).



Fig. 1. Map of 12 AmeriFlux sites (◇) and Walnut Creek (\*).

spatial distribution of humidity measurements is often too sparse for implementation of an interpolation scheme (New et al., 1999). Second, though relative humidity measurements are sometimes available, there is incomplete reporting on whether the record of relative humidity is an instantaneous observation or a daily average (New et al., 1999). This introduces error in the conversion of relative humidity to vapor pressure. Third, since VPD includes the effect of two temperatures (air temperature and dew point temperature), when biases are quite different for these two temperatures this can result in an even larger relative error in VPD estimates (Jolly et al., 2005). An alternative to interpolation is to find a variable strongly related to VPD that is measured extensively or even exhaustively. Elevation, though clearly related to air temperature through the lapse rate, is not closely related to VPD so elevation cannot be used directly in the estimation of VPD (Jolly et al., 2005).

In response to existing shortcomings and capitalizing on the availability of satellite data, Granger (1991) developed a technique to predict regional patterns of VPD from remotely sensed land surface temperature (LST). In comparison to

interpolation methods, estimating VPD from LST has at least two advantages. First, satellite observations have the potential to provide global coverage of LST from which to generate VPD estimates every day. The daily coverage is not realized because of the occurrence of clouds, but satellite LST is still far more dense and extensive than are ground-based measurements. Second, fewer calculations are required in a simple transfer function such as that from a regression than in an interpolation scheme. Granger (1991, 2000) proposed the following empirical model for daily VPD:

$$VPD = 0.668e^*(LST) - 0.015T_{lrm} - 0.278 \tag{1}$$

where  $e^*(LST)$  is saturation vapor pressure at the mean daily LST estimated from satellite data and  $T_{lrm}$  is long-term mean air temperature. Granger (1991, 2000) ascribed this simple relationship to a feedback link between land surface temperature and near-surface humidity (a function of water availability for evapotranspiration). The feedback link is inherent in the complementary relationship (Boucher, 1963): the summation

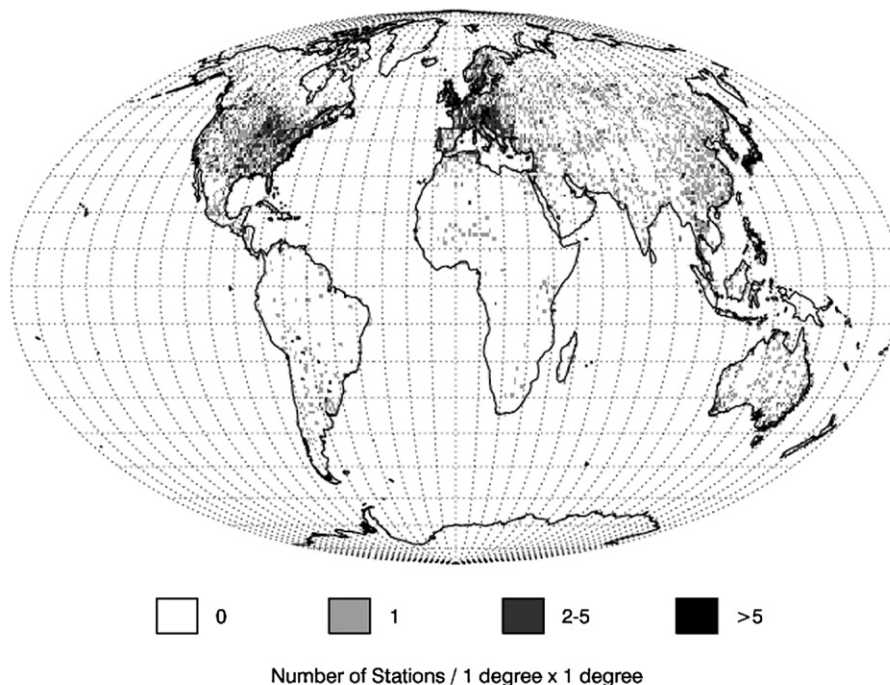


Fig. 2. Spatial distribution of GSSD stations. The gray scale shows the density of the stations (number of stations per 1 degree × 1 degree).

Table 1  
Summary of the data sources and scales used in the methodology

Step	VPD data source	Temporal resolution of VPD data	LST data source	Spatial resolution of LST data	Spatial extent	Temporal extent
1	From tower-based humidity and temperature measurements	Instantaneous	Tower-based infrared radiometer	Quasi-point	10 SMEX02 sites in Walnut Creek watershed	18 days 06/25/2002–07/12/2002
2	From tower-based humidity and temperature measurements	Daytime	Tower-based infrared radiometer	Quasi-point	10 SMEX02 sites in Walnut Creek watershed	18 days 06/25/2002–07/12/2002
3	From tower-based humidity and temperature measurements	Daytime	TERRA MOD11A2	1 km	12 Ameriflux sites in conterminous US north of 38° N	One year 2001
4	From min, max and dewpoint temperature measurements	8-day	TERRA MOD11A2	1 km	1079 GSSD sites in conterminous US	One year 2001
5	From min, max and dewpoint temperature measurements	8-day	TERRA and AQUA MOD11C2	0.05°	6069 global GSSD sites	8 days 08/5/2004–08/12/2004

of actual evapotranspiration and potential evapotranspiration is equal to twice the equilibrium evapotranspiration. That is, under a wide variety of climatological conditions over a region without abrupt environmental discontinuities, actual and potential evapotranspiration are linked. The complementary relationship theory has been examined and validated in many climatic regions (e.g., Brutsaert & Stricker, 1979; Hobbins et al., 2001; Morton, 1983), though the underlying theory remains controversial (McNaughton & Spriggs, 1989). Assumptions of the complementary relationship include (i) an equilibrium state between the land and the atmosphere, (ii) no advection of energy, and (iii) sufficient land surface moisture to maintain the connection between land and the atmosphere via evaporation. A linear relationship between VPD and  $e^*(LST)$  can fail to materialize under conditions when these assumptions are not met, for example, when the soil surface becomes very dry. Appendix A contains further details on how the feedback link leads to linearity between these two variables under a range of conditions.

Our objective in this study is to test a Granger-type linear model at a number of temporal and spatial resolutions to gain an understanding of how well the simple relationship may hold for application in regional and global ecosystem modeling. Our approach differs from prior research in significant technical and conceptual aspects. A technical aspect is the use of the LST product (Wan et al., 2004) from the Moderate Resolution Imaging Spectroradiometer (MODIS) instruments carried on the TERRA (morning overpass) and AQUA (afternoon overpass) satellites. MODIS data represent key advantages in comparison to the previously used Advanced Very High Resolution Radiometer (AVHRR) including 1) highly regular satellite overpass times obviating the orbital drift corrections needed for AVHRR (Lakshmi & Zehrhuhs, 2002), 2) availability of atmospheric water vapor information from MODIS spectral bands to increase the accuracy of LST retrieval (Wan & Li, 1997), 3) physically-based emissivity estimates from seven MODIS spectral bands (Wan et al., 2002) and 4) better cloud screening. Conceptually, we examine the theoretical principles at multiple measurement resolutions and extents; at an intensively instrumented site, widely distributed flux tower sites across a continent, and additional sites distributed globally. While we do not expect the models to be scale invariant given the spatial heterogeneity of surface temperature and the non-linear dependence of saturation vapor pressure on surface

temperature, we are interested in investigating how well a linear model shape is preserved over multiple scales. If linear models are useful at multiple scales, this supports the robustness of the feedback link concept as a basis for VPD estimation.

## 2. Data

We investigated relationships between VPD and  $e^*(LST)$  at a variety of different temporal and spatial resolutions. These included instantaneous VPD ( $VPD_{ins}$ ) to confirm the land–atmosphere coupling at short time scales, daytime-average VPD ( $VPD_{day}$ ) to test how well a single LST observation in the diurnal cycle can represent the daytime average critical for ecosystem modeling, and an 8-day average of daytime-average VPD ( $VPD_{8day}$ ) corresponding to the frequency of MODIS LST product availability.

### 2.1. Instantaneous and daytime VPD and LST from SMEX02 sites

We obtained VPD and LST data from 12 flux towers in the Soil Moisture Experiments in 2002 (SMEX02) at Walnut Creek near Ames, Iowa (Fig. 1) to examine the relationship between ground-based measurements of  $VPD_{ins}$  and  $e^*(LST)$ . The objectives of SMEX02 were to extend instrument observations and algorithms to a broader range of vegetation conditions, validate land surface parameters retrieved from satellite microwave sensors and to evaluate new instrument technologies for soil moisture remote sensing. Two types of crop canopies comprised the landcover on

Table 2  
Slopes and intercepts of the regression models fit to the training data for each step of the methods

Step	Slope	Intercept	RMSE	MAE
1 (10:30 am)	.321	–.241	.318	.257
1 (1:30 pm)	.383	–.287	.346	.277
2	.321	–.255	.331	.263
3	.391	–.028	.385	.274
4	.353	.154	.373	.254
5 (Terra)	.341	.198	.338	.252
5 (Aqua)	.270	.305	.322	.247

Root-Mean-Square-Error (RMSE) and Mean Absolute Error (MAE) from the test data for each step.

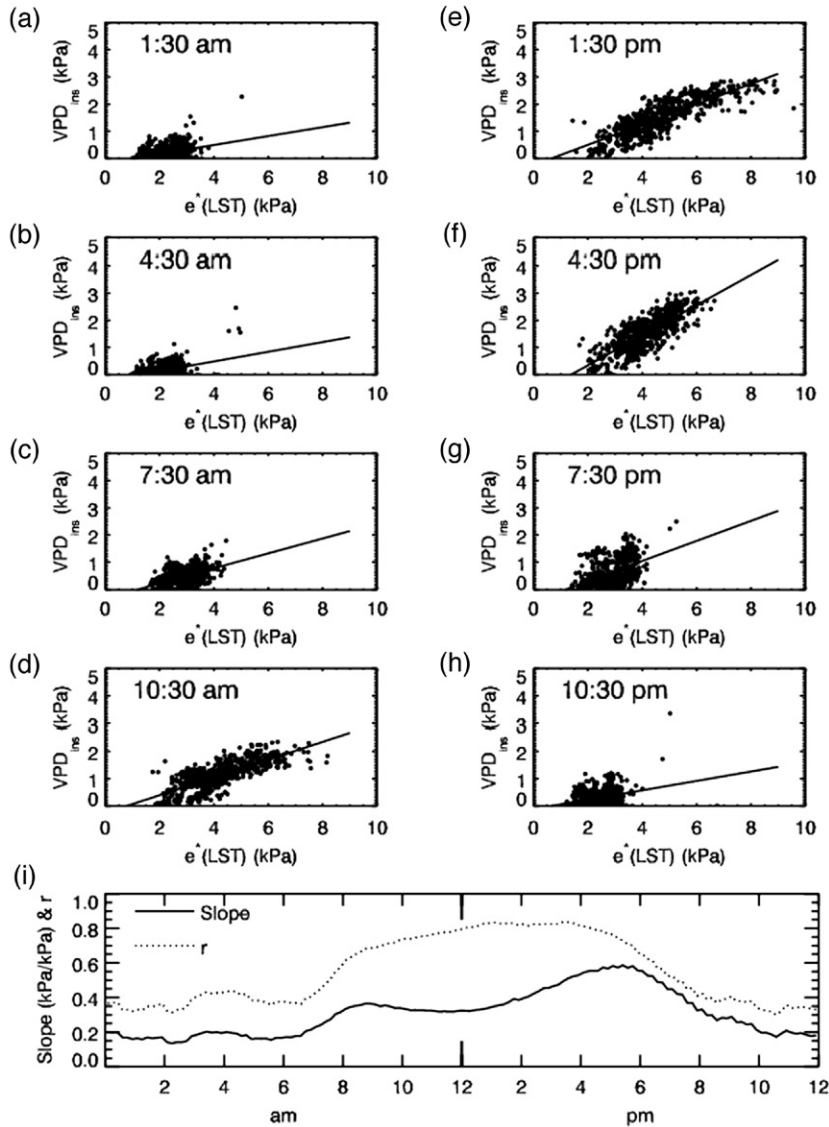


Fig. 3. Scatterplots between  $e^*(LST)$  derived from ground-based radiometers and  $VPD_{ins}$  for every 3 h [a–h] and time-series of slope and correlation coefficient ( $r$ ) [i] in Walnut Creek. Times are Central Daylight Time. Straight lines in the scatterplots [a–h] are linear regression lines.

the sites — corn and soybean. During the experiment, radiometric surface temperature on the sites was measured every 10 min by infrared sensors suspended on towers about 5 m above ground level over corn and about 2.5 m above ground level over soybean (Jackson & Cosh, 2003). Air temperature ( $T_a$ ) and vapor pressure ( $e_a$ ) were measured at 1.5 m above the canopy and used to calculate  $VPD_{ins}$ :

$$VPD_{ins} = e^*(T_a) - e_a. \quad (2)$$

$VPD_{day}$  was calculated as the average  $VPD_{ins}$  when solar radiation was greater than 0. Two of the twelve sites were deleted from the analysis because of an anomalous trend in VPD at one site (suspected to be caused by sensor bias) and unusual “spikes” in VPD at another site. Data representing either corn or soybean landcover were available from June 25, 2002 to July 12, 2002.

## 2.2. 8-day average VPD from AmeriFlux sites

We used AmeriFlux data (Baldocchi et al., 2001) from 12 sites (Fig. 1) over 2001. AmeriFlux is a network of tower platforms and instrumentation that provides continuous observations of ecosystem-level exchanges of  $CO_2$ , water, energy and momentum over daily, seasonal, and annual time scales based on the eddy-covariance flux approach. At the 12 sites, air temperature and vapor pressure were measured from towers above the vegetation canopy every 30 min and used with Eq. (2) to calculate  $VPD_{ins}$ .  $VPD_{day}$  was calculated as the average  $VPD_{ins}$  when solar radiation was greater than 0. Averaging half-hourly  $VPD_{ins}$  data provided a more direct method of estimating  $VPD_{day}$  than the common method of using maximum temperature, minimum temperature and average humidity.  $VPD_{day}$  values were averaged over every non-overlapping 8-day period over the year to calculate  $VPD_{8day}$ .

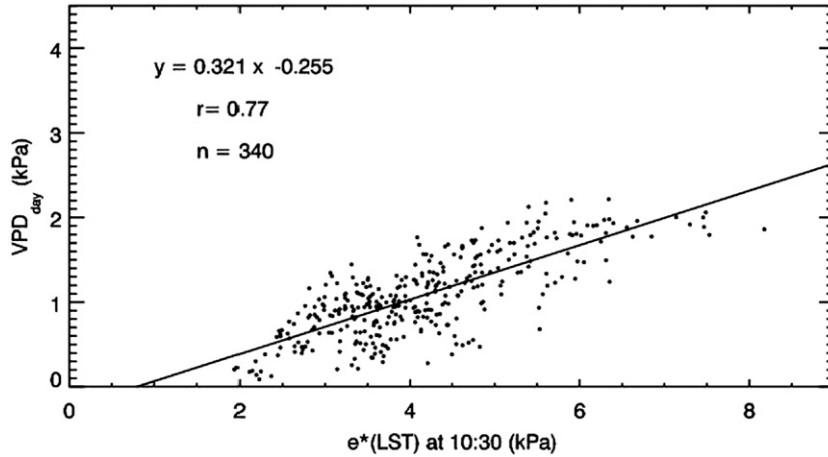


Fig. 4.  $VPD_{day}$  versus ground-based  $e^*(LST)$  at 10:30 am local time in Walnut Creek. The straight line is a linear regression line fit to the training data.

2.3. 8-day average VPD from GSSD stations

Daily dew point and minimum and maximum air temperatures from the 2001 Global Surface Summary of Day (GSSD) data version 6 produced by the National Climatic Data Center (NCDC) were used to estimate  $VPD_{day}$ . An assumption of sinusoidal variation of air temperature over the day is made to estimate current temperature at each hour:

$$T_t = \frac{T_{max} - T_{min}}{2} \sin\left(\frac{2\pi}{24}t - \frac{\pi}{2}\right) + \frac{T_{max} + T_{min}}{2} \quad (3)$$

where  $T_t$  is air temperature at time  $t$  (hour). Daytime VPD is then estimated by integrating the estimated difference between vapor pressure at each hour and saturation vapor pressure from the dewpoint over daylight hours

$$VPD_{day} = \frac{1}{12} \int_6^{18} \{e^*(T_t) - e^*(T_{dew})\} dt. \quad (4)$$

Eq. (4) was evaluated using Simpson’s Rule. We believe the errors introduced by this method are less than 200 Pa on a daily basis under clear sky conditions (Running et al., 1987). Values from Eq. (4) were averaged to produce a  $VPD_{8day}$  estimate for

every non-overlapping 8-day period over 2001. From the uneven network of GSSD stations (Fig. 2), we selected stations with less than 20% missing data that were not on small islands. In the conterminous US, 1079 stations met these criteria and 6069 met them globally. They are most densely concentrated in the eastern US and Europe but available on all continents except for Antarctica.

2.4. LST from the MODIS 11 product

We obtained 1 km Collection 4 TERRA MOD11 A2, representing land surface temperature, at AmeriFlux and conterminous US GSSD stations. MOD11 A2, calculated using the generalized split window technique (Wan & Dozier, 1996), is the 8-day average of cloud free daily MOD11 A1 data. Collection 4 data are the products generated using the best algorithms available as of 2004. For GSSD stations outside the US, we used the 0.05 degree TERRA and AQUA MOD11 C2 product. MOD11 C2 represents the 8-day average of cloud free daily MOD11 C1 data derived from 5 km MOD11 B1 data (Wan & Li, 1997). MOD11 LST is estimated in various landcover types with accuracy to within 1 K (Wan et al., 2002, 2004). To avoid cloudy or otherwise contaminated observations, we only

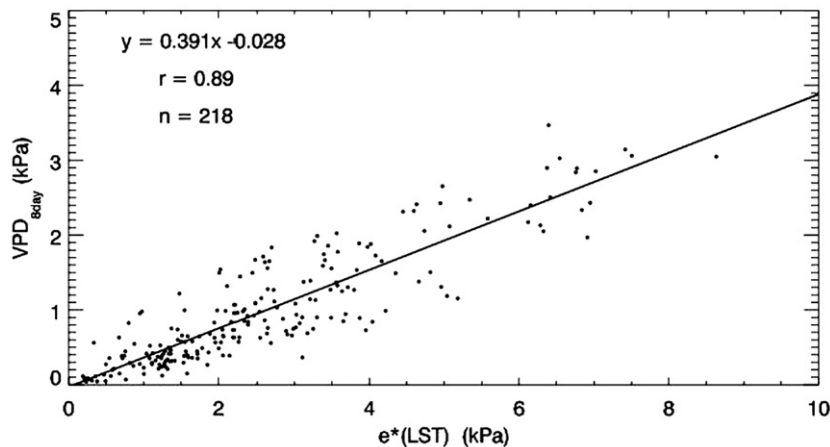


Fig. 5.  $VPD_{8day}$  versus MOD11-based  $e^*(LST)$  at AmeriFlux sites in 2001. The straight line is a linear regression line fit to the training data.

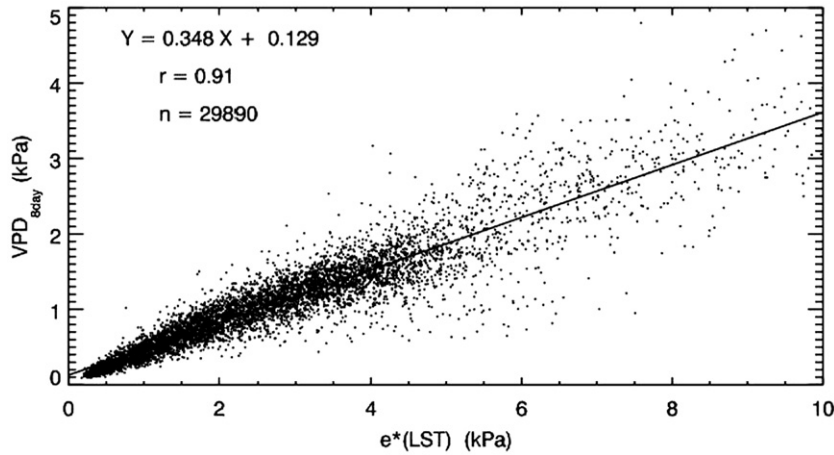


Fig. 6. GSSD  $VPD_{8day}$  versus MOD11-based  $e^*(LST)$  in the conterminous US for 2001. The straight line is the linear regression line fit to the training data.

used LST data with quality control flags set to 00 (highest quality).

### 3. Methods

#### 3.1. Model development

We modeled the relationships between ground-based measurements  $e^*(LST)$  and VPD as well as satellite-derived  $e^*(LST)$  at a number of scales. We pursued the following five steps with the available data. In all steps, we used the following equation to calculate saturation vapor pressure:

$$e^*(T) = 0.6107e^{17.38T/239.0+T} \quad (5)$$

where  $e^*(T)$  is given in kPa and  $T$  (LST when using MODIS data) is given in °C (Abbott & Tabony, 1985). The data sources

and scales used in each step are summarized in Table 1. The five steps were:

- (1) Examine the relationship between instantaneous VPD and saturation vapor pressure based on in-situ measured LST at Walnut Creek. We modeled the relationships between  $VPD_{ins}$  measured at the Walnut Creek towers versus  $e^*(LST)$  calculated from the 5 m-high radiometers every 3 h to observe diurnal variations of the feedback link.
- (2) Examine the relationship between daytime average VPD and measured LST at Walnut Creek. We modeled the relationship between  $VPD_{day}$  estimated at the Walnut Creek towers versus  $e^*(LST)$  measured from the 5 m-high radiometers at 10:30 am local time.
- (3) Examine the relationship between 8-day average VPD and MODIS-based LST at AmeriFlux sites. In a more spatially-distributed analysis, we modeled the relationship

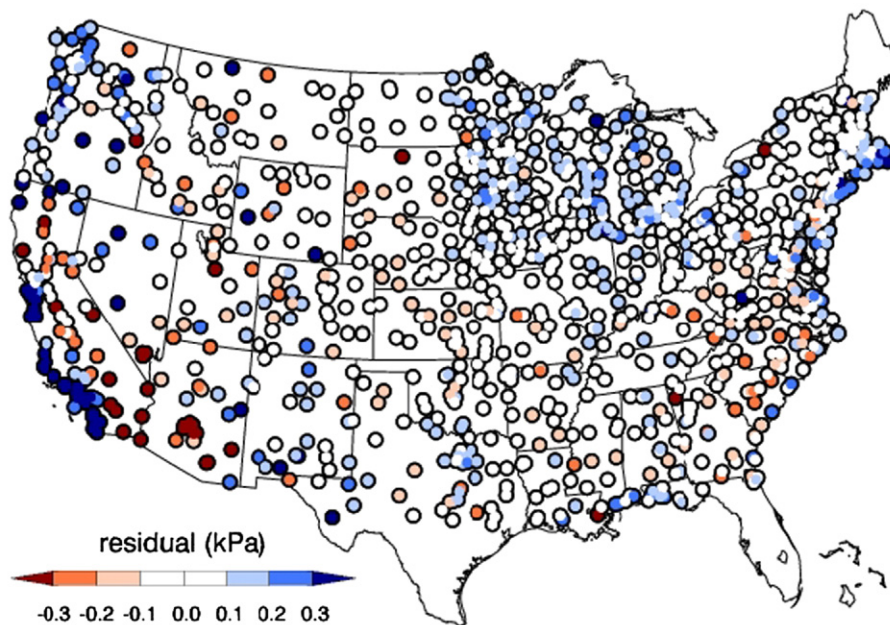


Fig. 7. Spatial distribution of the residuals of the regression line from step 4 at GSSD stations in the conterminous US.

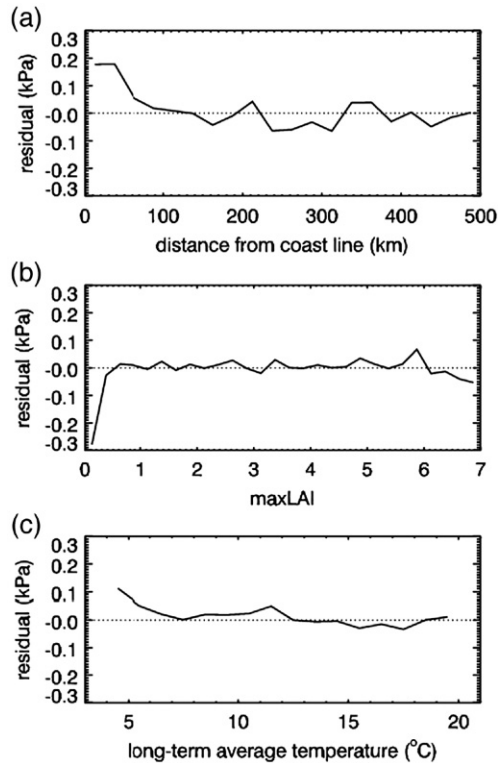


Fig. 8. (a) Average residual from the regression line versus distance from the nearest coastline. (b) Average residual from the regression line versus annual maximum LAI. (c) Average residual from the regression line versus long-term average temperature.

between  $VPD_{8day}$  from Ameriflux data versus the 1 km TERRA MOD11 A2-based  $e^*(LST)$  at 10:30 am local time at the 12 Ameriflux sites.

- (4) Examine the relationship between 8-day average VPD and MODIS-based LST at GSSD sites in the conterminous US. We modeled the relationship of GSSD-derived estimates of  $VPD_{8day}$  for US locations in 2001 versus the 1 km TERRA MOD11 A2-based  $e^*(LST)$ .
- (5) Examine the relationship between 8-day average VPD and MODIS-based LST at GSSD sites around the globe.

We modeled the relationship of GSSD-derived estimates of  $VPD_{8day}$  for global locations for a single composite period (August 5 to August 12) in 2004 versus the 0.05° TERRA and AQUA MOD11 C2.

### 3.2. Error evaluation

We used data splitting to assess the regression models for steps 2–5 above. In each case, two-thirds of the data chosen at random from the complete set were used as a training set to estimate the parameters of a linear regression model. The one-third of the data withheld from the training set was used for testing the model and estimating error. Errors are expressed as Root-Mean-Squared-Error (RMSE)

$$RMSE = \sqrt{\frac{1}{n} \sum_i^n (y_i - f(x_i))^2} \quad (6)$$

and Mean Absolute Error (MAE)

$$MAE = \frac{1}{n} \sum_i^n |y_i - f(x_i)| \quad (7)$$

where  $y_i$  is the  $i$ th observed test sample value,  $n$  is the number of test sample values and  $f(x_i)$  is the estimated  $i$ th value.

### 3.3. Tests in specific regions

As the above steps rely mainly on data from moist temperate sites in the US or Europe, where station density is high, we examined  $e^*(LST)$  versus  $VPD_{8day}$  for a tropical and a semi-arid site. We applied the model developed in step 4 to GSSD data from Porto Velho (8.76° S, 63.91° W) in the tropical Amazon and Kurnool (15.80° N, 78.06° E) in semi-arid India.

Furthermore, to compare patterns of spatial variability from the MODIS-based  $e^*(LST)$  method with traditional interpolation techniques, we generated a  $VPD_{8day}$  surface for April 23 to April 29, 2001 using the model developed in step 4 with MOD11 A2  $e^*(LST)$  for the state of California. We also interpolated

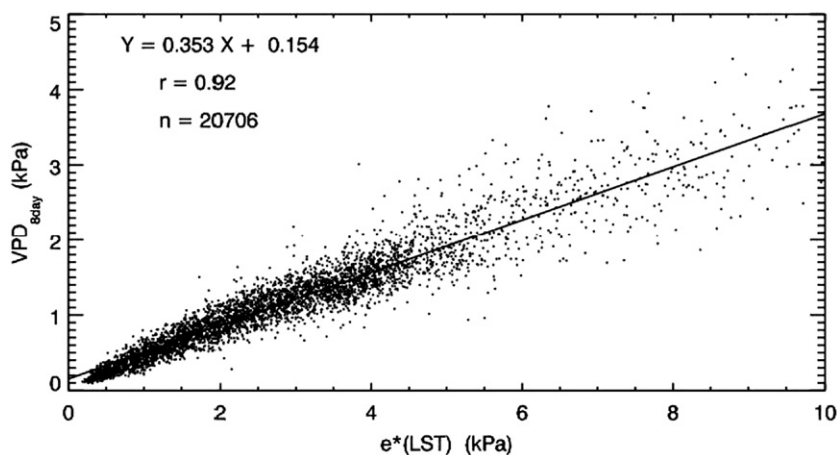


Fig. 9. GSSD  $VPD_{8day}$  versus MOD11-based  $e^*(LST)$  in the conterminous US for 2001. The straight line is the linear regression line fit to the training data. Data from stations within 50 km from coastlines or with less than 0.5 annual maximum LAI are excluded.

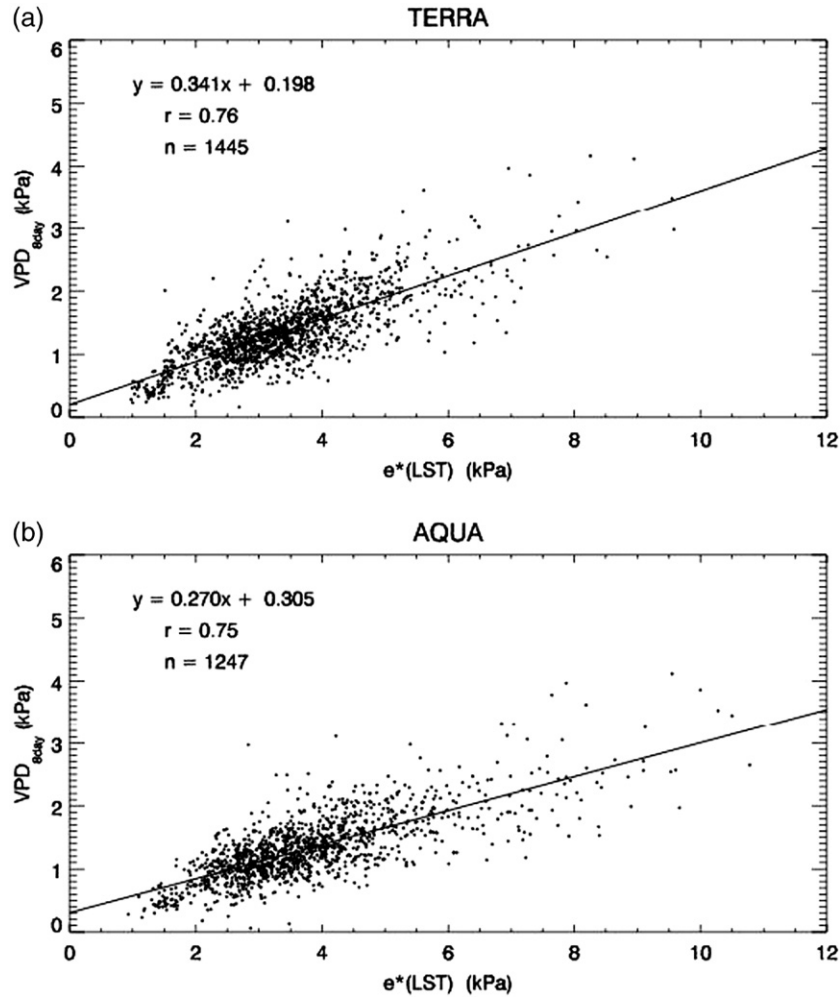


Fig. 10. GSSD  $VPD_{8day}$  versus (a) MOD11  $e^*(LST)$  from TERRA and (b) MOD11  $e^*(LST)$  from AQUA for all global stations with leaf area index greater than 0.5 for the DOY 217 to 224 composite period.

daily station data from the NCDC (with elevation adjustment) for the same region using ordinary kriging.

#### 4. Results

Parameters of the linear models fit to the training data from steps 1 through 5 and errors calculated from the test data are listed in Table 2.

##### 4.1. Tower-based $e^*(LST)$ versus $VPD_{ins}$ and $VPD_{day}$ (steps 1 and 2)

The data from the in-situ infrared sensor measurements at Walnut Creek showed that linear relationships between  $e^*(LST)$  and VPD existed for both  $VPD_{ins}$  (Fig. 3) and  $VPD_{day}$  (Fig. 4). Linear relationships between  $e^*(LST)$  and  $VPD_{ins}$  were observed from 8:00 am to 6:00 pm Central Daylight Time (CDT). At night, due to the small range of both VPD and LST, the correlation coefficient between  $e^*(LST)$  and  $VPD_{ins}$  was small. In the daytime, the slope of the linear regression line increased steadily from noon to 5:00 pm CDT. The difference in thermal inertia between the land surface and the atmosphere would be expected

to lead to increasing slopes as the land surface responds more slowly than the atmosphere to increasing insolation, causing LST to rise more slowly than VPD. Despite the change of slope, these results show that the instantaneous feedback link is active during the day, including at the overpass times of TERRA (10:30 am local time) and AQUA (1:30 pm local time). The daytime average VPD,  $VPD_{day}$ , at the Walnut Creek towers was linearly related to  $e^*(LST)$  at 10:30 am (Fig. 4) with a MAE of .26 kPa (Table 2), suggesting that  $VPD_{day}$  may be estimated with only an instantaneous observation of surface temperature at 10:30 am local time, the overpass time of the TERRA satellite.

##### 4.2. MODIS-based $e^*(LST)$ versus $VPD_{8day}$

###### 4.2.1. AmeriFlux sites (step 3)

A linear relationship was also found between MOD11 A2  $e^*(LST)$  and AmeriFlux  $VPD_{8day}$  (Fig. 5), with a MAE of 0.27 kPa.

###### 4.2.2. GSSD stations in the conterminous US (step 4)

The analysis of 2001  $e^*(LST)$  and  $VPD_{8day}$  for the conterminous US showed similar results to the Walnut Creek

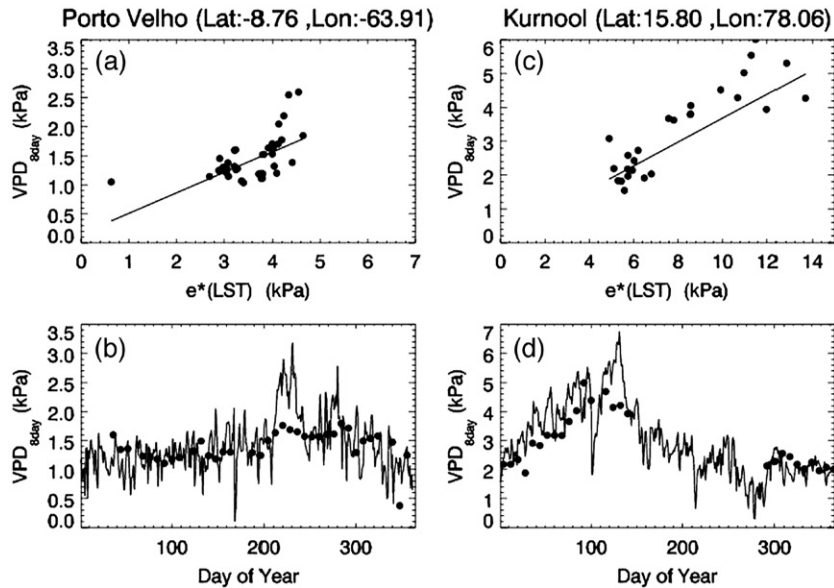


Fig. 11. Tests at Porto Velho in the Amazon (a and b) and at Kurnool in India (c and d). (a) and (c) are plots of  $VPD_{8day}$  against MODIS-based  $e^*(LST)$  and the straight line is from Eq. (8). (b) and (d) are time series of observed  $VPD_{8day}$  (line) from the GSSD station record and estimated  $VPD_{8day}$  (filled circles) from MOD11 LST data.

and AmeriFlux analyses: a clear linear relationship between MODIS-based  $e^*(LST)$  and  $VPD_{8day}$  (Fig. 6) with 0.25 kPa MAE (Table 2). In contrast to the scatterplots in Figs. 4 and 5 where residuals appear to support homoskedasticity, residuals increased with increasing  $e^*(LST)$ . When the residuals are mapped to their locations (Fig. 7), it is apparent that there are geographical clusters of stations that have particularly high or low residuals. Along coastal California, Washington and New England, VPD residuals are high, indicating that the best-fit linear model would overestimate VPD at these locations. A plot of the residuals versus distance from coastlines (Fig. 8a) shows that the regression line overestimates VPD within about 50 km from coastlines. Low residuals occurred in the arid region of California and Arizona (Fig. 7). Those regions are characterized by low values of annual maximum Leaf Area Index (LAI) as represented by the MODIS 15 LAI product (Knyazikhin et al., 1999). Fig. 8b shows apparent underestimation for stations that have maximum LAI less than 0.5.

Since Granger's model (1991, 1997) included a dependency on long-term temperature, we looked at regression residuals at the GSSD stations versus long-term average temperature (Fig. 8c). The long-term average temperature was calculated as the yearly average from 1980 to 2005 using GSSD records. There was no obvious trend with long-term average temperature (Fig. 8c) nor was any latitudinal temperature gradient evident in the model residuals (Fig. 7). The scatter of points (Fig. 6) shows a slight curvilinear shape at low values of  $e^*(LST)$ . Overestimates when long-term average temperature was below 6 °C (Fig. 8c) were caused by the non-zero intercept of the regression line resulting from the choice of a linear model. Though a  $T_{lim}$  term was used in Granger (1991, 2000), the coefficient on this term was very small.

A new model was fit to the training data excluding the locations within 50 km of the coast and locations with MODIS LAI < 0.5 (Fig. 9)

$$VPD_{8day} = 0.353e^*(LST(10 : 30am)) + 0.154. \quad (8)$$

#### 4.2.3. GSSD stations globally (step 5)

For the global GSSD stations from August 5 to August 12 in 2004,  $VPD_{8day}$  was linearly related to MOD11 C2-based  $e^*(LST)$  from both TERRA and AQUA platforms (Fig. 10). The MAE calculated on the test data was 0.25 kPa for both TERRA and AQUA, a similar magnitude of error as found with the models developed in previous steps. We note that the slope from TERRA data (0.341) was greater than the slope for AQUA data (0.270), and both slopes were smaller than slopes found in steps 3 and 4. A reduction in slope might be expected when pixel size increases because of the reduction in variance of the  $x$ -axis variable caused by spatial averaging. Part of the reduction in slope when comparing the results of step 5 with those of steps 3 and 4 may be due to this effect.

#### 4.3. Results of tests in specific regions

Application of Eq. (8) to the tropical Porto Velho and semi-arid Kurnool resulted in RMSE values of .35 and .72 respectively and MAE values of .27 and .60 respectively (Fig. 11a and c). The estimates as a time series showed generally good agreement with some error during anomalous weather events (Fig. 11b and d). In Porto Velho, Eq. (8) simulated the overall seasonal variation of  $VPD_{8day}$  well even though the variability of  $VPD_{8day}$  was low (0 – 3.5 kPa). However, the short dry period from DOY 210 to 250 was not well represented. In

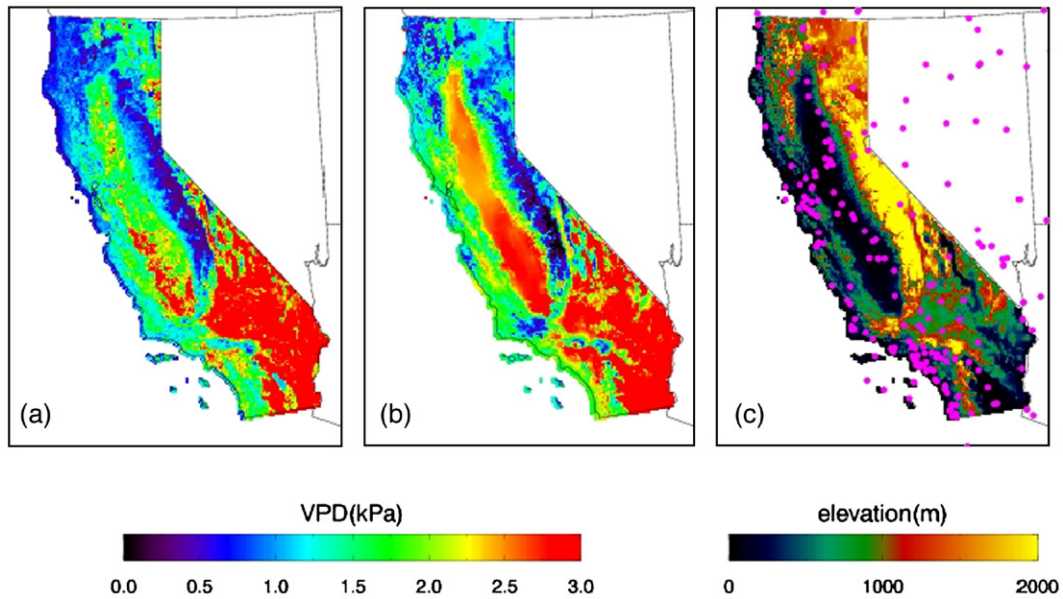


Fig. 12. Spatial patterns of VPD in the state of California estimated with (a) MODIS-based  $e^*(LST)$  and (b) ordinary kriging with elevation adjustment for DOY 113 to 120 in 2001. Those elevation and station data used to calculate (b) are shown in (c).

Kurnool, Eq. (8) captured the larger seasonal variation of  $VPD_{8day}$  estimated from station data. The Asian Monsoon creates pronounced dry and wet seasons in Kurnool; severe dry conditions from DOY 120 to 140 that likely violate the feedback link hypothesis (Appendix A) led to  $VPD_{8day}$  underestimation. LST estimates from MODIS have higher uncertainty under dry conditions (Wan et al., 2002). An additional plausible explanation of the underestimation when LST values are high is that errors in LST estimation are magnified when used in the exponential function  $e^*(LST)$  because of the law of uncertainty propagation. In the rainy season from DOY 150 to 300, cloud contamination prevented  $VPD_{8day}$  estimation.

The MOD11 A2-based model from Eq. (8) resulted in extensive  $VPD_{8day}$  heterogeneity in the central valley of California (Fig. 12a). Kriging (Fig. 12b), in which most variation was generated by elevation change (Fig. 12c), showed a highly constrained  $VPD_{8day}$  range. Thus, even in one of the more densely instrumented areas of the world, station density does not capture the probable large spatial heterogeneity of VPD. This result indicates that satellite-based VPD estimation may be especially useful for capturing spatial details.

## 5. Discussion

We have developed and tested very simple regression models for estimating VPD at a variety of spatial and temporal resolutions from remotely sensed  $e^*(LST)$  without recourse to ancillary information such as land cover, leaf area index, or soil properties. VPD estimation from remote sensing is not new, but our approach includes multi-scale analysis from point to globe that has only recently become possible and avoids problematic treatment of variables such as total precipitable water and

vertical temperature profiles (Czajkowski et al., 2002). We used MODIS-derived products for the first time, which facilitated regional and global tests.

MAEs observed from test data in the five analysis steps tended to be of a similar magnitude, roughly 15–20% of the mean VPD value. Similarly, RMSEs were fairly consistent across models, roughly 20–25% of the mean. Jolly et al. (2005) had a similar goal of mapping regional VPD, but used interpolation methods to predict values between measurement stations. In that study, interpolated VPD surfaces resulted in a cross-validation MAE of 0.14 kPa from inverse distance weighting, 0.17 kPa from a truncated Gaussian filter and 0.29 kPa from ordinary kriging for the conterminous United States. Cross validation errors and those found with a large sample of test data, as in this study, are not directly comparable, and so the relative accuracy of the two cannot be judged without a sufficiently large set of test data that interpolation methods could be tested with in parallel with the linear models developed here.

Users should be aware of temporal and spatial resolution issues inherent in these analyses. Note that different temporal and spatial resolutions of VPD and LST in the five steps resulted in different slopes and intercepts. This is not unexpected, for in order for an algorithm to be scale invariant, two conditions must be met: (1) the algorithm functions must be linear and (2) the input variables must also be scale invariant; that is, the variable value at a pixel can be calculated as the area-weighted average of the sub-pixel patch-scale values (Hall et al., 1992). The  $e^*(LST)$  method satisfies condition 2 but, due to inclusion of the exponential function of saturation vapor pressure, condition 1 is violated. Any algorithm describing VPD as a function of  $e^*(LST)$  will therefore not be scale invariant.

The lack of scale invariance helps explain why the model parameters in Table 2 are different than those in the model developed by Granger (Eq. (1)). Granger used satellite-derived LST with different spatial resolutions than MODIS and used estimates of daily average LST rather than instantaneous LST. We ignored the problems inherent in extrapolating instantaneous LST estimates to daily average values (Jin & Dickinson, 1999; Jin, 2004). In addition, we did not find that long-term air temperature helped explain VPD and so did not use the  $T_{\text{ltm}}$  term used by Granger. Other reasons, such as undiscovered biases in VPD estimation using station data or errors in LST estimation using MODIS might also help account for differences.

There are basic scale-mismatch problems inherent in steps 2–5. That is, the spatial and temporal resolutions of the  $e^*(\text{LST})$  and VPD variables differ. For example, in all of these steps, LST is measured instantaneously and VPD is a temporal average over a day or an 8-day period. Therefore, there is an aspect of the simple linear models that incorporates a change-of-scale. Those wishing to employ a linear model should give careful consideration to the temporal and spatial resolutions of the data they have available and at what resolutions they wish to predict. The theoretical relationships derived in the Appendix are for quasi-point and instantaneous spatial and temporal resolutions and so cannot be used directly to develop models relevant to area- and time-integrated variables.

Averaging ten-minute (in the case of Walnut Creek) or half-hourly (in the case of Ameriflux)  $\text{VPD}_{\text{ins}}$  data provide a more direct method of estimating  $\text{VPD}_{\text{day}}$  than the common method of using maximum temperature, minimum temperature and average humidity. The VPD data from flux tower stations are likely to be more accurate than VPD estimated at GSSD stations using temperature data. AmeriFlux sites represent ideal conditions for the  $e^*(\text{LST})$  method for two reasons: (1) they are designed to observe  $\text{CO}_2$  and latent heat fluxes for specific landcovers and consequently their footprints are relatively spatially homogeneous and (2) humidity is observed above the canopy, the assumed location in most ecosystem models. These considerations may suggest the use of the equation developed in step 3. However, Ameriflux data do not represent a global range of land surfaces and is a small data set limiting the amount of model evaluation that can be done. These factors should be considered when selecting a model from those developed here.

Cloud cover limits the operational use of our method. We developed our models using 8-day LST products derived from daily products produced only in clear-sky pixels, as determined by the 99% confidence level from the MODIS cloud mask (Ackerman et al., 1998). Nonetheless, sub-pixel broken clouds are known to contaminate the LST products (Wan et al., 2002), which may in turn create uncertainty in calculated slope values.

The method has potential to obtain spatial patterns of VPD for broad regions, but caution should be applied near coastlines and in very arid regions where the annual maximum LAI is less than 0.5. Sea breezes may partly explain the overestimation along the coastlines since they represent water advection onto land. Further analysis concentrated on the interaction between

the land surface and atmosphere adjacent to oceans could prove informative. In arid regions where annual maximum LAI is less than 0.5, the coupling between land and the atmosphere is dominated by sensible heat flux over long periods of time, conditions that tend to violate the equilibrium that this method is based on.

## 6. Conclusions

We revisited the  $e^*(\text{LST})$  method of predicting VPD proposed by Granger (1991, 2000) for regional and global scales. Our approach represents an empirical investigation of the explanatory power of simple linear relationships for describing a key variable used in many ecosystem models using currently available satellite-based measurements. It hinges on the instantaneous measure of land surface temperature captured by polar-orbiting satellites. We note the general robustness of this approach as expressed in linear relationships observed in data from ground observations in SMEX02, Ameriflux, an extensive network of surface weather stations, and satellite remote sensing from MODIS. The errors in this analysis were of similar magnitude to results from interpolation methods, making our approach attractive in regions with sparse weather observations. However, this method overestimates VPD within 50 km of coastlines and underestimates VPD in very arid, non-vegetated regions. Also, the uncertainty is greater when VPD is high.

While use of both TERRA and AQUA data will increase the chances of obtaining cloud-free data (Wan et al., 2004), operational implementation of the  $e^*(\text{LST})$  method for near real-time ecological monitoring and modeling (e.g. Nemani et al., 2003) is fundamentally limited by cloud contamination. The strengths of the technique, computational simplicity and the ability to represent fine spatial detail, though, are well suited to couple with observational networks. Similarly, ground observations could be ingested in an assimilation technique to adjust any emergent biases in VPD from  $e^*(\text{LST})$ . This scheme would combine synoptic satellite capabilities with critical ground based observations to represent VPD variability for modeling and monitoring applications quickly, reliably, and accurately. Satellite data are becoming widely available, often within minutes of data collection, through the internet as well as from inexpensive receivers. Simple algorithms such as our VPD method could be easily implemented on inexpensive computers such that satellite observations can be translated to useful information regarding such as estimates of evapotranspiration by using ecosystem models, if possible, with the correction of biases using ground-observation data.

## Acknowledgements

This research was supported by a doctoral fellowship to HH from the Japan Society for the Promotion of Science (JSPS). Funding from NASA's Science Mission Directorate supported the participation of RRN, MAW (NNG04G043G), JLD, and SWR. We would like to acknowledge Ameriflux and SMEX02 for archiving and providing some of the data used in this

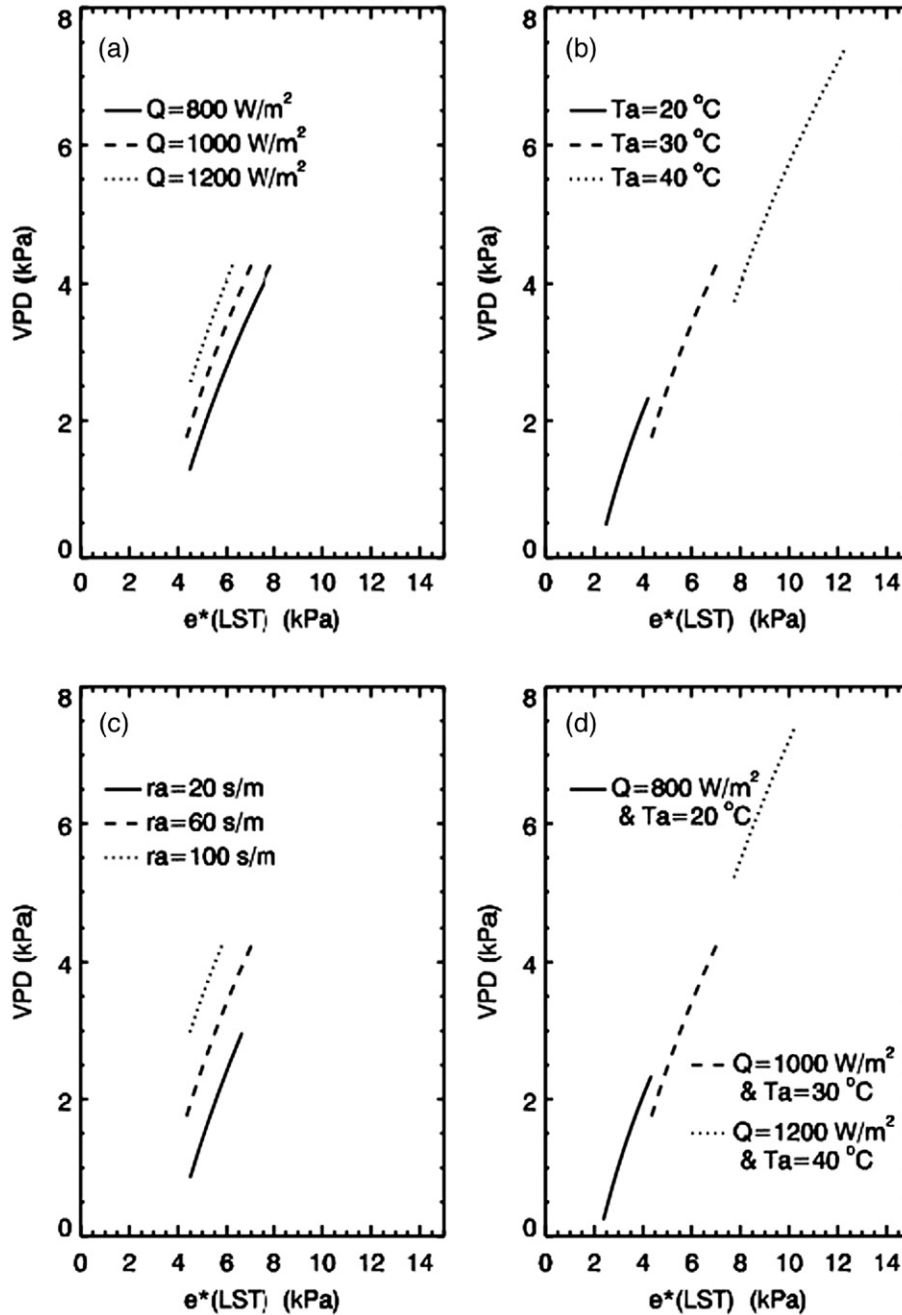


Fig. A1. Results of numerical experiments to investigate the relationship between VPD and  $e^*(LST)$ . Experiment (a) changed the input energy ( $Q=800, 1000,$  and  $1200 \text{ W m}^{-2}$ ). Experiment (b) changed the air temperature ( $T_a=20, 30,$  and  $40 \text{ }^\circ\text{C}$ ). Experiment (c) changed the aerodynamic resistance ( $r_a=20, 60,$  and  $100 \text{ s m}^{-1}$ ). Experiment (d) changed both the input energy and the air temperature ( $Q=800 \text{ W m}^{-2}$  and  $T_a=20 \text{ }^\circ\text{C}$ ,  $Q=1000 \text{ W m}^{-2}$  and  $T_a=30 \text{ }^\circ\text{C}$ , and  $Q=1200 \text{ W m}^{-2}$  and  $T_a=40 \text{ }^\circ\text{C}$ ).

study. Discussions with Dr. Granger helped to articulate this study from local to global scales.

**Appendix A. Theory of the linear relationship between VPD and  $e^*(LST)$**

In this section, we explain the linear relationship between VPD and  $e^*(LST)$  from the feedback link. We begin with the complementary relationship (Boucher, 1963)

$$E_a = 2E_e - E_p \tag{A1}$$

where  $E_a$  is the actual evapotranspiration,  $E_e$  is the equilibrium evapotranspiration, and  $E_p$  is the potential evapotranspiration. The excess evaporation energy ( $E_e - E_a$ ) due to the unavailability of water is added to the equilibrium evaporation energy ( $E_e$ ) as the potential evaporation energy ( $E_p$ ), or  $E_e - E_a = E_p - E_e$  (this is equivalent to Eq. (A1)). We modeled the feedback link using the advection–aridity model (Brutsaert & Stricker, 1979) which estimates  $E_p$  by Eq. (A2) (Penman, 1948) and  $E_e$  by Eq. (A3) (Priestley & Taylor, 1972).

$$\lambda E_p = \frac{\Delta}{\Delta + \gamma} (R_n - G) + D \tag{A2}$$

$$\lambda Ee = \alpha \frac{\Delta}{\Delta + \gamma} (R_n - G) \quad (\text{A3})$$

where  $\alpha$  is a constant value of 1.28,  $\Delta$  is the slope of the saturation vapor pressure deficit at the air temperature,  $\gamma$  is the psychrometric constant,  $D$  is the drying power of air,  $\lambda$  is the latent heat of vaporization,  $R_n$  is the net radiation, and  $G$  is the ground heat flux. We calculated  $D$  from VPD (cf. Nishida et al., 2003) such that

$$D = \rho C_p \frac{\text{VPD}}{(\Delta + \gamma)r_a} \quad (\text{A4})$$

where  $r_a$  is aerodynamic resistance,  $\rho$  is the density of air, and  $C_p$  is the specific heat capacity of air. VPD is  $e^*(T_a) - e_a$ , where  $T_a$  is the air temperature and  $e_a$  is the vapor pressure of air. For other constraining conditions, we used the energy budget Eq. (A5) and the radiation budget Eq. (A6).

$$R_n - G = H + \lambda E a \quad (\text{A5})$$

$$R_n = (1 - a)S\downarrow + L\downarrow - L\uparrow \quad (\text{A6})$$

where  $H$  is the sensible heat flux,  $a$  is the surface albedo,  $S\downarrow$  is the downward shortwave radiation,  $L\downarrow$  is the downward longwave radiation and  $L\uparrow$  is the upward longwave radiation. We calculated  $H$  as:

$$H = \rho C_p \frac{T_s - T_a}{r_a} \quad (\text{A7})$$

where  $T_s$  is surface temperature. We expressed  $L\uparrow$  as a function of  $T_s$

$$L\uparrow = \varepsilon \sigma T_s^4 \quad (\text{A8})$$

where  $\sigma$  is the Stefan–Boltzmann constant,  $5.67 * 10^{-8} \text{ W m}^{-2} \text{ K}^{-4}$ , and  $\varepsilon$  is surface emissivity (set to 1). We defined the input energy  $Q$  as

$$Q = R_n - G + L\uparrow = (1 - a)S\downarrow + L\downarrow - G. \quad (\text{A9})$$

Rearranging, the energy balance equation becomes

$$Q = H + \lambda E a + L\uparrow. \quad (\text{A10})$$

Using four numerical experiments (Table A1) and the system of equations described above, we developed a theoretical model space to explain the relationship between VPD and  $e^*(\text{LST})$ . We implemented single parameter variations for  $Q$  (experiment A),  $T_a$  (experiment B), and  $r_a$  (experiment C). In the diurnal cycle,  $Q$  and  $T_a$  tend to vary in tandem, so in experiment D we changed both  $Q$  and  $T_a$  proportionally. We ignored unrealistic results for clear days (negative sensible or latent heat flux); these occurred in conditions too humid or too dry to explain evapotranspiration by the complementary relationship.

For each experiment, we found the almost linear relationship between VPD and  $e^*(\text{LST})$  proposed by Granger (Fig. A1). High LST leads to high  $H$  and low  $Ea$  from the energy budget Eq. (A5). The complementary relationship between  $Ea$  and  $Ep$  (Eq. (A1)) results in high  $Ep$ . This, in turn, results in high VPD

as per Eq. (A4). Based on these simulations, the following principles emerged. Larger  $Q$  decreases  $e^*(\text{LST})$  since more energy is available for latent heat flux (Fig. A1a). Due to the exponential function of saturation vapor pressure with temperature, higher air temperature widens the range of the linear relationship (Fig. A1b). Higher  $r_a$  leads to smaller  $e^*(\text{LST})$  because, at constant  $Ee$ , higher  $r_a$  implies smaller  $Ep$  and larger  $Ea$  such that less energy is partitioned to  $H$  (Fig. A1c). When co-varied realistically, the effects of  $Q$  and  $T_a$  produce a highly linear relationship between VPD and  $e^*(\text{LST})$ . Although  $r_a$  has some impact on the coefficients of the regression equation, these results provide the theoretical basis for our proposition that a linear function may be used to estimate VPD from  $e^*(\text{LST})$ .

We note that these numerical experiments demonstrate an instantaneous linearity between VPD and  $e^*(\text{LST})$ . Modeling the relation between daytime average VPD and  $e^*(\text{LST})$  is less straightforward because of the complication of diurnal variation in the terms of Eqs. (A1)–(A10).

**Table A1**

Description of the variables ( $Q$ ,  $T_a$ , and  $r_a$ ) for each numerical experiment

Experiment	$Q$ ( $\text{W m}^{-2}$ )	$T_a$ ( $^{\circ}\text{C}$ )	$r_a$ ( $\text{s m}^{-1}$ )
A	800, 1000, 1200	30	60
B	1000	20, 30, 40	60
C	1000	30	20, 60, 100
D	800, 1000, 1200	20, 30, 40	60

## References

- Abbott, P. F., & Tabony, R. C. (1985). The estimation of humidity parameters. *Meteorological Magazine*, 114, 49–56.
- Aber, J. D., Reich, P. B., & Goulden, M. L. (1996). Extrapolating leaf  $\text{CO}_2$  exchange to the canopy: A generalized model of forest photosynthesis compared with measurements by eddy correlation. *Oecologia*, 106, 257–265.
- Ackerman, S. A., Strabala, K. I., Menzel, W. P., Frey, R. A., Moeller, C. C., & Gumley, L. E. (1998). Discriminating clear sky from clouds with MODIS. *Journal of Geophysical Research*, 103, 32141–32158.
- Baldocchi, D. D., Falge, E., Gu, L., Olson, R., Hollinger, D. Y., Running, S. W., et al. (2001). FLUXNET: A new tool to study the temporal and spatial variability of ecosystem-scale carbon dioxide, water vapor, and energy flux densities. *Bulletin of the American Meteorological Society*, 82, 2415–2434.
- Boucher, R. J. (1963). Evapotranspiration réelle et potentielle, signification climatique. *Proc. of the Berkeley Symposium. Int. Ass. Sci. Hydrol., Belgium* (pp. 134–142).
- Brooker, P. (1979). Kriging. *Engineering and Mining Journal*, 180, 148–153.
- Brutsaert, W., & Stricker, H. (1979). An advection–aridity approach to estimate actual regional evapotranspiration. *Water Resources Research*, 15, 443–450.
- Czajkowski, K. P., Goward, S. N., Shirey, D., & Walz, A. (2002). Thermal remote sensing of near-surface water vapor. *Remote Sensing of Environment*, 79, 253–265.
- Granger, R. J. (1991). *Evaporation from natural nonsaturated surfaces*. Ph.D thesis, University of Saskatchewan, 141 pp.
- Granger, R. J. (1997). Comparison of surface and satellite-derived estimates of evapotranspiration using a feedback algorithm. In G. W. Kite, A. Pietroniro, & T. J. Schultz (Eds.), *Applications of remote sensing in hydrology, Proceedings of the Third International Workshop NHRI Symposium, vol. 17* (pp. 71–81). Greenbelt, Maryland: NASA Goddard Space Flight Center.
- Granger, R. J. (2000). Satellite-derived estimates of evapotranspiration in the Gediz basin. *Journal of Hydrology*, 229, 70–76.

- Hall, F. G., Huemmrich, K. F., Goetz, S. J., Sellers, P. J., & Nickeson, J. E. (1992). Satellite remote sensing of surface energy balance: Success, failure, and unresolved issues in FIFE. *Journal of Geophysical Research*, 97(D17), 19061–19089.
- Hobbins, M. T., Ramírez, J., Brown, T. C., & Claessens, L. H. J. M. (2001). The complementary relationship in estimation of regional evapotranspiration: The complementary relationship areal evapotranspiration and advection–aridity models. *Water Resources Research*, 37, 1367–1388.
- Hutchinson, M. F., & Gessler, P. E. (1994). Splines — More than just a smooth interpolator. *Geoderma*, 62, 45–67.
- Jackson, T., & Cosh, M. (2003). *SMEX02 tower-based radiometric surface temperature, Walnut Creek, Iowa*. Boulder, CO: National Snow and Ice Data Center, Digital media.
- Jin, M. (2004). Analysis of land skin temperature using AVHRR observations. *Bulletin of the American Meteorological Society*, 85, 587–600.
- Jin, M., & Dickinson, R. E. (1999). Interpolation of surface radiative temperature measured from polar orbiting satellites to a diurnal cycle 1. Without clouds. *Journal of Geophysical Research*, 104, 2105–2116.
- Jolly, W. M., Graham, J. M., Michaelis, A., Nemani, R. R., & Running, S. W. (2005). A flexible, integrated system for generating meteorological surfaces derived from point sources across multiple geographic scales. *Environmental Modelling and Software*, 20, 873–882.
- Knyazikhin, Y., Glassy, J., Privette, J. L., Tian, Y., Löttsch, A., Zhang, Y., et al. (1999). MODIS Leaf Area Index (LAI) and Fraction of Photosynthetically Active Radiation Absorbed by Vegetation (FPAR) Product (MOD15) Algorithm Theoretical Basis Document. [http://modis.gsfc.nasa.gov/data/atbd/atbd\\_mod15.pdf](http://modis.gsfc.nasa.gov/data/atbd/atbd_mod15.pdf)
- Lakshmi, V., & Zehrhuhs, D. (2002). Normalization and comparison of surface temperatures across a range of scales. *IEEE Transactions of Geoscience and Remote Sensing*, 40, 2636–2646.
- McNaughton, K. G., & Spriggs, T. W. (1989). An evaluation of the Priestley and Taylor equation and the complementary relationship using results from a mixed-layer model of the convective boundary layer. In T. A. Black, D. L. Spittlehouse, M. D. Novak, & D. T. Price (Eds.), *Estimation of Areal Evaporation* (pp. 89–103). Wallingford, U.K: IAHS Press.
- Morton, F. I. (1983). Operational estimates of areal evapotranspiration and their significance to the science and practice of hydrology. *Journal of Hydrology*, 66, 1–76.
- Nemani, R. R., White, M., Pierce, L., Votava, P., Coughlan, J., & Running, S. W. (2003). Biospheric monitoring and ecological forecasting. *Earth Observation Magazine*, 12, 1560–1563.
- New, M., Hulme, M., & Jones, P. (1999). Representing twentieth-century space–time climate variability. Part I: Development of a 1961–90 mean monthly terrestrial climatology. *Journal of Climate*, 12, 829–856.
- Nishida, K., Nemani, R. R., Running, S. W., & Glassy, J. M. (2003). An operational remote sensing algorithm of land surface evaporation. *Journal of Geophysical Research*, 108(D9), 4270. doi:10.1029/2002JD002062
- Penman, H. L. (1948). Natural evaporation from open water, bare soil, and grass. *Proceedings of the Royal Society of London, Series A*, vol. 193 (pp. 120–146).
- Priestley, C. H. B., & Taylor, R. J. (1972). On the assessment of surface heat flux and evaporation using large-scale parameters. *Monthly Weather Review*, 100, 81–92.
- Running, S. W., Nemani, R. R., & Hungerford, R. D. (1987). Extrapolation of synoptic meteorological data in mountainous terrain and its use for simulating forest evapotranspiration and photosynthesis. *Canadian Journal of Forest Research*, 17, 472–483.
- Thiessen, A. H. (1911). Precipitation averages for large areas. *Monthly Weather Review*, 39, 1082–1084.
- Thornton, P. E., Running, S. W., & White, M. A. (1997). Generating surfaces of daily meteorological variables over large regions of complex terrain. *Journal of Hydrology*, 190, 214–251.
- Van Wijk, M. T., Dekker, S. C., Bouten, W., Bosveld, F. C., Kohsiek, W., Kramer, K., et al. (2000). Modeling daily gas exchange of a Douglas-fir forest: Comparison of three stomatal conductance models with and without a soil water stress function. *Tree Physiology*, 20, 115–122.
- Wan, Z., & Dozier, J. (1996). A generalized split-window algorithm for retrieving land-surface temperature from space. *IEEE Transactions on Geoscience and Remote Sensing*, 34, 892–905.
- Wan, Z., & Li, Z. -L. (1997). A physics-based algorithm for retrieving land-surface emissivity and temperature from EOS/MODIS data. *IEEE Transactions on Geoscience and Remote Sensing*, 35, 980–996.
- Wan, Z., Zhang, Y., Zhang, Q., & Li, Z. -L. (2002). Validation of the land-surface temperature products retrieved from Terra Moderate Resolution Imaging Spectroradiometer data. *Remote Sensing of Environment*, 83, 163–180.
- Wan, Z., Zhang, Y., Zhang, Q., & Li, Z. -L. (2004). Quality assessment and validation of the MODIS global land surface temperature. *International Journal of Remote Sensing*, 25, 261–274.
- Waring, R. H., & Running, S. W. (1998). *Forest ecosystems: Analysis at multiple scales*. San Diego: Academic Press.
- Watson, D. F., & Philip, G. M. (1985). A refinement of inverse distance weighted interpolation. *Geo-processing*, 2, 315–327.
- White, M. A., Thornton, P. E., Running, S. W., & Nemani, R. R. (2000). Parameterization and sensitivity analysis of the BIOME-BGC terrestrial ecosystem model: Net primary production controls. *Earth Interactions*, 4, 1–85.